# Lattice dynamics of $AgGaSe_2$. I. Experiment

J. Camassel
*Groupe d'Etude des Semiconducteurs, Université des Sciences et Techniques du Languedoc, 34095 Montpellier CEDEX, France*

L. Artus
*Institut de Cìencia de Materials de Barcelona (ICMAB), Consell Superior d'Investigacions Cientifiques (CSIC), calle/Marti i Franquès, 08028 Barcelona, Spain*

J. Pascual
*Departament Fisica i Institut de Cìencia de Materials de Barcelona (ICMAB), Consell Superior d'Investigacions Cientifiques (CSIC), Universitat Autònoma de Barcelona, 08193 Bellaterra, Spain*

(Received 16 August 1989)

We report a detailed investigation of the infrared and Raman activity of $AgGaSe_2$. Performing, first, infrared studies in the spectral range 15–500 $cm^{-1}$, both at room and at liquid-helium temperature, we could identify all $\Gamma_4$ ($\mathbf{E}\|\mathbf{c}$) and $\Gamma_5$ ($\mathbf{E}\perp\mathbf{c}$) vibrational modes predicted by group-theory arguments. This includes, at low energy, the complete series of folded-acoustic components resolved for the first time and second, at higher energy, a nearly degenerate $\Gamma_5$ doublet at 249.5–252.1 $cm^{-1}$. All frequencies obtained in that way were independently checked by performing, under nearly resonant conditions, Raman investigations at 77 K. We could then identify four additional modes: $1\Gamma_1$ and $3\Gamma_3$. Our experimental results demonstrate that all zone-center modes can be grouped in three energy bands: First, within a very narrow energy range centered around 250 $cm^{-1}$ are four modes ($1\Gamma_3+1\Gamma_4+2\Gamma_5$); next, in an intermediate region extending from 180 to 135 $cm^{-1}$ are five modes ($1\Gamma_1+1\Gamma_3+1\Gamma_4+2\Gamma_5$); and, finally, at much lower energy the dispersion of the acoustic branches gives, in the range 25–85 $cm^{-1}$, another series of four modes which are associated with $1\Gamma_3+1\Gamma_4+2\Gamma_5$ symmetry.

## I. INTRODUCTION

Silver gallium diselenide ($AgGaSe_2$) is a well-known chalcopyrite compound which, like many other ternary analogs of the II-VI and III-V binary materials, has long been investigated for linear and nonlinear optical properties.[1] For instance, within the same family, $CuInSe_2$ has been recently reported as the strongest absorbing semiconductor known under sunlight[2] and both $ZnGeP_2$ and $CdGeAs_2$ are efficient second-harmonic generators and parametric infrared mixers.[3]

Despite this long-range technical interest, not much is known about the lattice dynamics of ternary $ABC_2$ compound semiconductors, in general, and $AgGaSe_2$, in particular. From the simplest viewpoint, $AgGaSe_2$ is the ternary analog of the fictitious compound $Cd_{0.5}Zn_{0.5}Se$ (cubic). This point is now well documented[4] and simple structural connections link the chalcopyrites with the more standard family of ZnS-type materials. In the particular case of $AgGaSe_2$, every fictitious (averaged) $Zn_{0.5}Cd_{0.5}$ cation has been replaced, alternatively, by one heavier (silver) and a lighter (gallium) species to form interconnected "Ag—Se"-like and "Ga—Se"-like bonds. As a matter of fact, all peculiarities of the chalcopyrite compounds come from the relative ordering (and the nonequivalence) of these two different bonds: this is why they have long been considered for device applications in nonlinear optics. Unfortunately, this is also why they experience limited growth conditions.

## II. SYSTEMATICS OF $ABC_2$ SEMICONDUCTORS AND APPLICATION TO $AgGaSe_2$

The mixing of two cationic species induces first a change of space group from $T_d^2$ (or $F\bar{4}3m$), characteristic of cubic semiconductors with the ZnS-type structure), to the tetragonal space group $D_{2d}^{12}$ ($I\bar{4}2d$). For ideal (unrelaxed) chalcopyrite crystals the long dimension $c$ would be twice the cubic length. For real ternary crystals, however, there are structural modifications which affect this simple scheme. They come from the obvious requirement that the two different series of anion-cation distances have to match together. First is the so-called tetrahedral distortion. It is a weak displacement of anions, with respect to the ideal ZnS-type position ($a\sqrt{3}/4$) which can be characterized[4] by one single parameter $u$. It is such that

$$u-\tfrac{1}{4}=(d_{AC}^2-d_{BC}^2)/a^2$$

and correlates *only* with the change in first-nearest-neighbor distances $d_{AC}$ and $d_{BC}$, respectively. Second is the tetragonal compression which makes $c$ lower than the ideal ratio $c=2a$. For $AgGaSe_2$, these structural parameters have the following values:[3,4] $c/2a=\eta=0.896$ and $u=0.27$.

Because there are two different types of cations, and because the volume of the unit cell is four times larger than in a typical ZnS-type material, there is a four to one

 

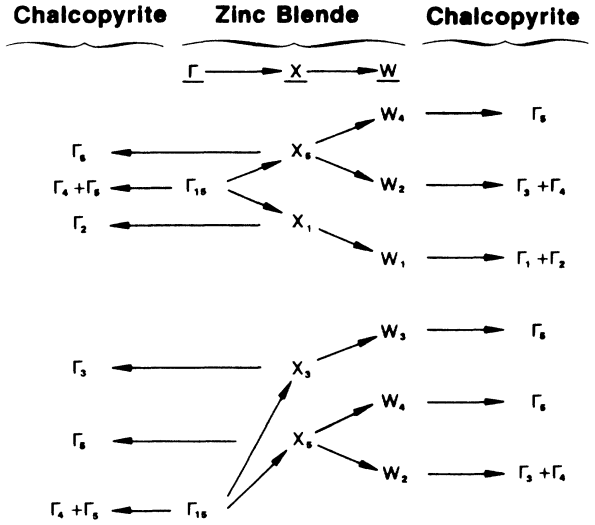


FIG. 1. Schematic drawing of the compatibility relations which link the vibrational modes of the chalcopyrites with respect to the corresponding ZnS-type material. Please notice how two $W$ representations at points $(0,2\pi/a,\pi/a)$ and $(2\pi/a,0,\pi/a)$ of the Brillouin zone have to match to give $\Gamma_1+\Gamma_2$ and $\Gamma_3+\Gamma_4$ partner modes. The related crystal-field splittings are indicative of the magnitude of the chalcopyrite distortion.

correspondence between the Brillouin zone (BZ) of the ideal chalcopyrite ($u=0$; $\eta=1$) and the BZ of the zinc-blende-structure semiconductor. As a matter of fact, all points labeled $X(0,0,2\pi/a)$, $W(0,2\pi/a,\pi/a)$, and $W(2\pi/a,0,\pi/a)$ fold back to the center of the Brillouin zone and correspond now, in the chalcopyrite structure, to zone-center ($\Gamma$-like) representations. For convenience, in the remaining part of this work, we shall call them $\Gamma[X]$ and $\Gamma[W]$, respectively. Moreover, since the chalcopyrite compounds crystallize with eight atoms per unit cell (two formula units), one expects 24 vibrational modes. In other words, since the cubic compounds only have six modes, six should be now folded $\Gamma[X]$ and 12 folded $\Gamma[W]$ components. In the tetragonal space group $D_{2d}^{12}$, at the center of the BZ, this reduces to

$$1\Gamma_1+2\Gamma_2+3\Gamma_3+4\Gamma_4+7\Gamma_5$$

where all $\Gamma_5$ modes are doubly degenerated and only one manifold, with symmetry $\Gamma_4+\Gamma_5$, originates from the $\Gamma_{15}$ optical mode of the equivalent cubic material.

In Fig. 1, we illustrate the compatibility relations which link the $\Gamma$, $X$, and $W$ branches of the starting material and, in Table I, we give the correspondence with the $\Gamma$ modes of the chalcopyrites. Notice that, every time, two $W$ representations at equivalent points $(0,2\pi/a,\pi/a)$ and $(2\pi/a,0,\pi/a)$ combine. This gives interesting features: (i) in the cases of $W_3$ and $W_4$, there appear only three degenerated modes with $\Gamma_5$ representations; (ii) in the case of $W_1$ and $W_2$, there appear both one series of nondegenerate $\Gamma_1+\Gamma_2$ and two series of nondegenerate $\Gamma_3+\Gamma_4$ partner modes, respectively. In that case, the magnitude of the corresponding splitting should be a direct measure of the chalcopyrite distortion induced upon the related ZnS-type material. We shall come back to this point later.

Not included in this figure is the long-range electrostatic interaction which splits, for the $\Gamma_4$ and $\Gamma_5$ modes, the longitudinal and transverse frequencies. This results in nine additional LO components which can be deduced from (i) the magnitude of the infrared oscillator strengths (LO-TO splitting) and (ii) specific selection rules observed in the Raman spectra.

Concerning the relative ordering of the different frequencies, we have to come back to the dispersion of the phonon branches in the related ZnS-type materials. The point is that very few reports deal with the $W$ points of the Brillouin zone. As a matter of fact, experimental

TABLE I. Combination of the ZnS-type modes in $AgGaSe_2$, activity and related selection rules. Within this simple scheme, all modes should be grouped in three bands with (i) at high energy a group of six modes with $\Gamma_3+2\Gamma_4+3\Gamma_5$ symmetry, (ii) in the intermediate range, a group of three optically active components with symmetry $\Gamma_1+\Gamma_3+\Gamma_5$, and (iii) at low energy, a last group of four modes with symmetry $\Gamma_3+\Gamma_4+2\Gamma_5$. This is opposite to the experimental findings.

| ZnS-type material | Chalcopyrite | Activity | Selection rules |
|---|---|---|---|
| $W_4(0,2\pi/a,\pi/a)+W_4(2\pi/a,0,\pi/a)$ | | | |
| $X_5(0,0,2\pi/a)$ | $3\Gamma_5$ | ir; $R$ | E⊥C; $xz,yz$ |
| $[\Gamma_{15}]_{opt}$ | $2\Gamma_4$ | ir; $R$ | E∥C; $xy$ |
| $W_2(0,2\pi/a,\pi/a)+W_2(2\pi/a,0,\pi/a)$ | $\Gamma_3$ | $R$ | $(x^2-y^2)$ |
| $X_1(0,0,2\pi/a)$ | $2\Gamma_2$ | Silent | |
| $W_1(0,2\pi/a,\pi/a)+W_1(2\pi/a,0,\pi/a)$ | $\Gamma_1$ | $R$ | $(x^2+y^2);z^2$ |
| $X_3(0,0,2\pi/a)$ | $\Gamma_3$ | $R$ | $(x^2-y^2)$ |
| $W_3(0,2\pi/a,\pi/a)+W_3(2\pi/a,0,\pi/a)$ | $\Gamma_5$ | ir; $R$ | E⊥C; $xz$; $yz$ |
| $W_4(0,2\pi/a,\pi/a)+W_4(2\pi/a,0,\pi/a)$ | | | |
| $X_5(0,0,2\pi/a)$ | $2\Gamma_5$ | ir; $R$ | E⊥C; $xz$; $yz$ |
| $W_2(0,2\pi/a,\pi/a)+W_2(2\pi/a,0,\pi/a)$ | $\Gamma_4+\Gamma_3$ | (ir; $R$)+$R$ | (E∥C;$xy$)+$(x^2-y^2)$ |
| $(\Gamma_{15})_{ac}$ | $(\Gamma_4+\Gamma_5)_{ac}$ | ac | |

values can only be found in inelastic neutron scattering experiments reported for (i) the group-IV elemental semiconductors Ge (Ref. 5) and Si,[6] and (ii) the prototype III-V compound: GaAs.[7] In each case, the overall bending of the dispersion curves in the $X-W$ direction indicates a hardening for the transverse optic and acoustic branches ($X_5$ to $W_2$ and $W_4$) and a softening for the longitudinal ones ($X_1$ to $W_1$ and $X_3$ to $W_3$). Indirect confirmation can be found in the second-order Raman spectra. See for instance, in the work of Ref. 8, the data reported for ZnSe. This is, in our case, of particular interest since ZnSe constitutes one of the two binary compounds associated with $AgGaSe_2$. The net consequence is that one expects first, at low energy, a group of four frequencies ($\Gamma_3+\Gamma_4+2\Gamma_5$) coming from the TA branch of the material; next, in the intermediate range, a group of five modes ($\Gamma_1+2\Gamma_2+\Gamma_3+\Gamma_5$) coming from various admixtures of acoustic (LA) and optic (LO) branches (this should be very sensitive to the details of the crystal structure), and finally, at high energy, a group of six modes ($\Gamma_3+2\Gamma_4+3\Gamma_5$) with very little dispersion.

On the experimental side, the few data that are available hardly reflect this simple scheme. The first experiments were conducted by Van der Ziel *et al.*[9] They performed Raman spectroscopy and used the 6471-Å line of a krypton-ion laser as exciting frequency. Working too far above band gap, they could only resolve a few, poorly identified, Raman-active components. Independently, Miller *et al.*[10] investigated the infrared activity and collected, in the spectral range 50–400 $cm^{-1}$, room-temperature reflectivity spectra. They found indication of 2 $\Gamma_4$ and 4 $\Gamma_5$ modes and discussed these results in terms of the folded-zone scheme. Starting from the results of a neutron-scattering experiment performed by Hennion *et al.*[11] for ZnSe, they proposed that the missing frequencies originated only from the low-energy acoustic branches. They were identified as (i) the low-energy $\Gamma_4$ mode (labeled $\Gamma_4[W_2]_{ac}$ in the remaining part of this work) and, (ii) two $\Gamma_5$ modes ($\Gamma_5[W_4]_{ac}$ and $\Gamma_5[X_5]_{ac}$). Later on, Kanellis and Kampas[12] repeated the experiments but got rather different features. Working in an extended range, from about 10 to 400 $cm^{-1}$, they could resolve a first low-energy $\Gamma_5$ component ($\Gamma_5[W_4]_{ac}$ mode) which appeared at about 80 $cm^{-1}$. However, they found also striking discrepancies in the high-energy range: they reported a close degeneracy of the $\Gamma_5[W_4]_{opt}$ mode with the dominant $\Gamma_5[\Gamma_{15}]$ feature (instead of a shift by 42 $cm^{-1}$, as reported in Ref. 10). To clear up this point, we have recently started a series of experiments in the range 50–400 $cm^{-1}$. At low energy, our preliminary data[13] showed the first indication of the third $\Gamma_4$ component ($\Gamma_4[W_2]_{ac}$) but no indication of the corresponding $\Gamma_5$ counterpart ($\Gamma_5[X_5]_{ac}$). It was expected to lie at lower energy and we could not resolve it. At higher energy, we supported the results of Ref. 12, and the near degeneracy of the $\Gamma_5[\Gamma_{15}]$ and $\Gamma_5[W_4]_{opt}$ modes but, again, no clear experimental resolution was possible.

In the present work, we have investigated in full detail the infrared and Raman activity of $AgGaSe_2$. In order to resolve the folded-acoustic branches, we have performed a series of transmission experiments, at about 20 K, in the spectral range 20–250 $cm^{-1}$. This gives unambiguous assignments for the energy position of both the $\Gamma_5[X_5]_{ac}$ and $\Gamma_4[W_2]_{ac}$ modes. Performing next reflectivity measurements at 20 K, we could resolve a clear doublet, with an energy separation close to 2.5 $cm^{-1}$. This corresponds to the high-energy $\Gamma_5[W_4]_{opt}$ and $\Gamma_5[\Gamma_{15}]$ components. Next, we have performed a series of least-mean-squares fits and deduced longitudinal and transverse frequencies for all infrared-active components. To compare with Raman data, we have collected a series of experimental spectra at 77 K and, to take as much advantage as possible of the selection rules, we have worked in the transparency region. All results obtained in this way agree with the infrared spectra and permitted us to achieve a complete assignment of the $\Gamma_1$, $\Gamma_3$, $\Gamma_4$(L), $\Gamma_4$(T), $\Gamma_5$(L), and $\Gamma_5$(T) Raman-active modes.

We have found three series of infrared and/or Raman-active frequencies. First, in the low-frequency range, are four modes of symmetry ($1\Gamma_3+1\Gamma_4+2\Gamma_5$) agreeing well with the folded-zone scheme. In this work, we shall identify them as $\Gamma_5[X_5]_{ac}$, $\Gamma_5[W_4]_{ac}$, $\Gamma_4[W_2]_{ac}$, and $\Gamma_3[W_2]_{ac}$. In the high-frequency range are again four modes (with symmetry $1\Gamma_3+1\Gamma_4+2\Gamma_5$) while we expected six. Two have obvious correspondence with the $\Gamma_{15}$ mode of the starting material and will be denoted $\Gamma_4[\Gamma_{15}]$ and $\Gamma_5[\Gamma_{15}]$. Two originate from the $W$ points of the unfolded BZ and will be denoted $\Gamma_3[W_2]$ and $\Gamma_5[W_4]$. Both missing modes have mixed, in an intermediate-frequency range, with the three active frequencies expected from the folded-zone scheme. This gives an intermediate series of five modes ($1\Gamma_1+1\Gamma_3+1\Gamma_4+2\Gamma_5$) which clearly sets the limits of this approximation and suggests a totally different viewpoint: because there are two different bonds, there are two different series of force constants. They correspond with light (heavy) cations beating against the common anion and, roughly speaking, span in the high- (intermediate-) frequency range.

In a next paper, hereafter referred to as Paper II, we shall discuss our data in the light of a simple Keating model,[14] as used by Martin[15] and Kane[16] for III-V materials. It was extended by Bettini[17] to the chalcopyrite structure and will permit us to get more quantitative information about the short-range interactions which rule a given vibrational mode. Starting from the folded-zone scheme, we add various interactions and see how they affect the description of vibrational modes in the high to intermediate regions.

## III. EXPERIMENTAL DETAILS

All crystals used in these experiments have been kindly provided to us by R. Feigelson, Center for Materials Research of Stanford University (Palo Alto, California). The samples used in the infrared experiments were cut in the form of thin platelets (about 1 mm thick) and included in their large face both **c** [001] and **a** [100] crystallographic directions. The samples used in the Raman experiments were also 1 mm thick and because large (001),

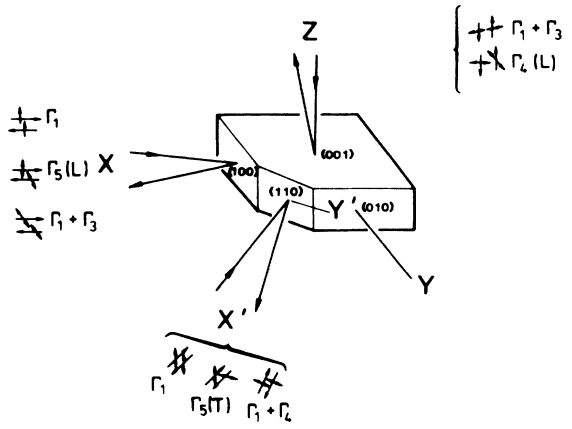


FIG. 2. Schematic illustration of the backscattering geometry used in the Raman experiments and related selection rules.

(100), and (110) faces have been used, we could observe, in the backscattering configuration, the *selective* excitation of the $\Gamma_1$, $\Gamma_1+\Gamma_3$, $\Gamma_4$(L), $\Gamma_4$(T), $\Gamma_5$(L), and, finally, $\Gamma_5$(T) components.

Our infrared apparatus has been already described[18] and the only modifications[19] concerned (i) the use of two germanium bolometers cooled down to liquid-helium temperature and (ii) the use of a helium exchange gas cryostat to cool down the samples and perform experiments at about 20 K. By carefully pumping on the helium bath, these bolometers allowed us to work in the spectral ranges 15–50 and 50–250 $cm^{-1}$, respectively.

As already said, our Raman spectra have been collected in the backscattering configuration, with all samples carefully polished with diamond paste and syton. A schematic illustration of the scattering geometry, together with the polarization of the incoming and outgoing beams, is shown in Fig. 2. The angle of incidence was about 20° and, using a Spex Industries double monochromator with standard photon counting techniques, the experimental resolution was typically 1.1 $cm^{-1}$.

At room temperature, using the 7525-Å line of a $Kr^+$-ion laser (Spectra-Physics, model 171) as exciting frequency, the corresponding photon energy (1.65 eV) was too close to band gap. In some cases, the samples were damaged. In order to increase the incident power, and to get a better signal to noise ratio, the band-gap energy was increased to about 1.83 eV, by keeping the samples immersed in a liquid-nitrogen bath.[20] However, the incident power was kept every time below 100 mW.

## IV. EXPERIMENTAL RESULTS

### A. Infrared-active modes

Shown in Fig. 3 are two different transmission spectra which both have been collected at 20 K with unpolarized light, but concern two different samples. In the first case [Fig. 3(a)] the sample thickness was about 5 mm. The corresponding spectrum reveals clearly an absorption feature, centered around 26 $cm^{-1}$. This is the low-energy

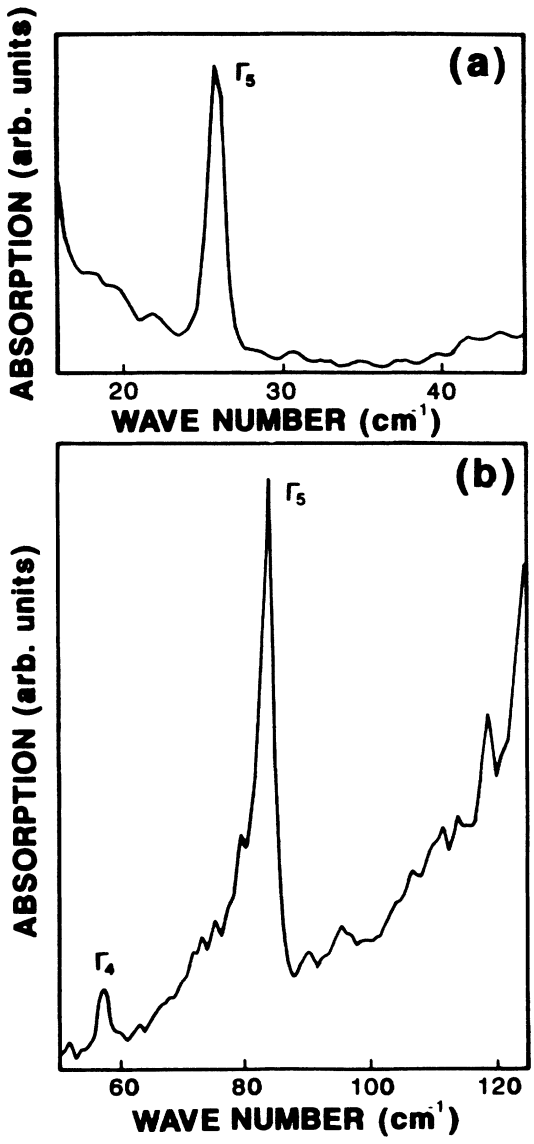


FIG. 3. Experimental transmission spectra obtained, at 20 K with unpolarized light, on two different samples. In the first case (a), the weak $\Gamma_5[X_5]_{ac}$ folded component is clearly found. In the second case (b), both $\Gamma_4[W_2]_{ac}$ and $\Gamma_5[W_4]_{ac}$ have been shown (see text).

$\Gamma_5$ mode which is resolved for the first time. It comes when folding the $[X_5]_{ac}$ acoustic branch. In Fig. 3(b), complementary data correspond to the range 50–125 $cm^{-1}$. They have been collected on a thinner sample (about 2 mm thick) and now two absorption features have been found. They manifest with different intensities. The first one is the small $\Gamma_4$ mode, which comes when folding to the center of the Brillouin zone the $[W_2]$ acoustic branch, the second is the $\Gamma_5[W_4]_{ac}$ component. The corresponding energy positions obtained from the data of Fig. 3 are 57 and 84 $cm^{-1}$, respectively, and agree well with previous identifications.[12,13] Finally, a strong absorption band appears above 100 $cm^{-1}$ and corresponds to the contribution of higher-frequency modes. Although

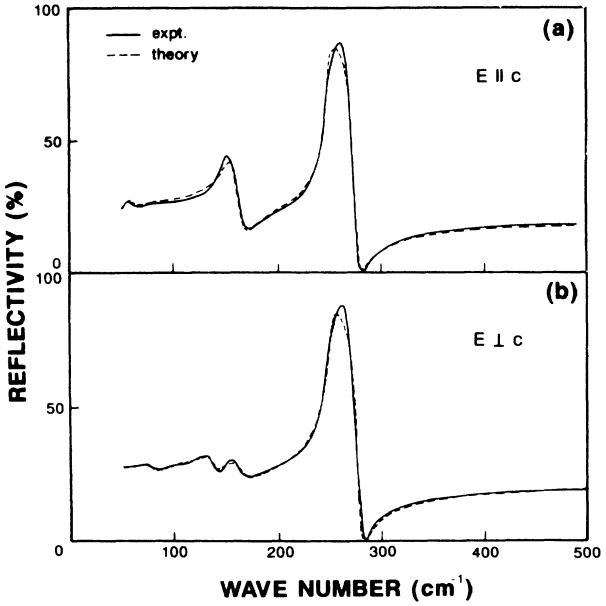


FIG. 4. Experimental reflectivity spectra (solid lines) and theoretical oscillator fits (dashed lines) obtained at room temperature in the two different configurations $\mathbf{E}\|\mathbf{c}$ and $\mathbf{E}\perp\mathbf{c}$.

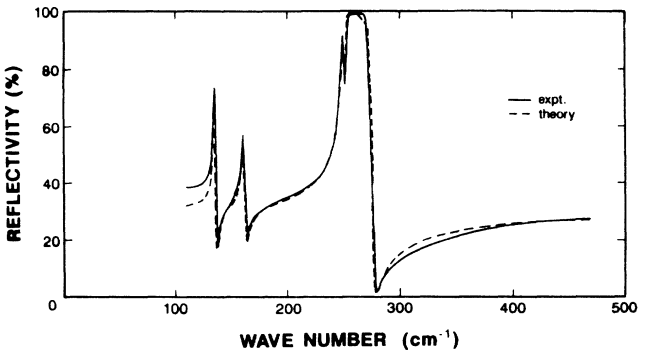


FIG. 5. Experimental reflectivity spectrum observed at 20 K in the polarization $\mathbf{E}\perp\mathbf{c}$ (solid line). The oscillator fit analysis (dashed line) gives for the two $\Gamma_5$ modes theoretical frequencies 249.5 (strong) and 252.1 (weak), respectively.

most have been identified from previous polarized reflectivity measurements,[10,12,13] for clarity, we display our experimental results in Fig. 4(a) ($\mathbf{E}\|\mathbf{c}$) and Fig. 4(b) ($\mathbf{E}\perp\mathbf{c}$), respectively.

Consider first Fig. 4(a). All experimental structures correspond now to $\Gamma_4$ frequencies. Qualitatively speaking, we notice an immediate discrepancy with respect to the folded-zone scheme: while we expected two bands, with two high-frequency modes and a low-frequency one, we find (i) a low-frequency component ($\Gamma_4[W_2]_{ac}$); (ii) a high-frequency component ($\Gamma_4[\Gamma_{15}]$); and (iii) a third mode which falls in an intermediate region. This is a first consequence of the bond alteration scheme which will be discussed at length in paper II. To get more quantitative information, we have performed an oscillator fit analysis,[19] using three independent frequencies and a least-mean-squares fit procedure. The resulting theoretical spectrum is shown as a dashed line in Fig. 4(a) and the corresponding parameters have been listed in Table II.

In Fig. 4(b), only four modes manifest and correspond with clear $\Gamma_5$ assignments. Taking account of the results of Fig. 3, we find two modes at low energy (below 100 $cm^{-1}$), while two modes appear in the intermediate-energy range (100–200 $cm^{-1}$); finally two modes, which should be found in the high-energy range, are not experimentally resolved. This, again, disagrees with the predictions of the folded scheme but confirms that one mode is not found using standard techniques. We have used our liquid-helium apparatus to perform additional experiments in this energy range. The results are shown in Fig. 5 (solid line) where, again, an oscillator fit analysis is displayed for the purpose of comparison (dashed line).

Because of the restricted aperture of the cryostat, we collected less intensity and only data in the range 100–500 $cm^{-1}$ could be Fourier transformed with a good signal to noise ratio. One dip is clearly revealed at 252.1

TABLE II. Oscillator fit parameters obtained in this work at (a) 20 K and (b) 300 K. All frequencies are given in $cm^{-1}$. The oscillator strengths and broadening parameters are reduced (dimensionless) quantities as defined in Ref. 19. Finally, labeled $(\ )_a$ are absorption data collected at 20 K.

| | Frequency ($cm^{-1}$) | | | | Oscillator strength | | Broadening parameters | |
|---|---|---|---|---|---|---|---|---|
| | TO | | LO | | | | | |
| | (a) | (b) | (a) | (b) | (a) | (b) | (a) | (b) |
| $\Gamma_4$ | $(57)_a$ | 62.5 | | 63 | | 0.093 | | 0.103 |
| | | 154.5 | | 165 | | 1.3 | | 0.095 |
| | | 249.5 | | 275.5 | | 1.338 | | 0.015 |
| $\Gamma_5$ | $(26)_a$ | | | | | | | |
| | $(84)_a$ | 79 | | 80 | | 0.212 | | 0.167 |
| | 135 | 135 | 136 | 137 | 0.30 | 0.376 | 0.004 | 0.101 |
| | 162 | 162.5 | 164 | 165 | 0.25 | 0.501 | 0.004 | 0.142 |
| | 249.5 | 248 | 276 | 278.5 | 1.8 | 0.909 | 0.003 | 0.018 |
| | 252.1 | 251 | | 250 | 0.2 | 0.750 | 0.001 | 0.016 |

$cm^{-1}$ which does not appear at room temperature. To avoid artifacts due to the finite incidence angle, we emphasize that a pure $s$ configuration was used.[21] However, there is no $\Gamma_4$(LO) frequency which, falling in this energy range, could couple to light. As a consequence, no finite incidence effects should be expected and we strongly believe that the small additional structure observed in this work is nothing but the missing $\Gamma_5$ frequency. Concerning the oscillator fit parameters listed in Table II, we emphasize that the magnitude of the theoretical structure displayed in this energy range is extremely sensitive to the energy difference which exists between the strong $\Gamma_5[\Gamma_{15}]$ mode (at 249.5 $cm^{-1}$) and the weak folded component (at 252.1 $cm^{-1}$). As a consequence the value quoted in this work (2.5 $cm^{-1}$) is certainly accurate within 0.5 $cm^{-1}$. Also interesting to discuss is the theoretical ratio of about 1:10 which connects both dimensionless oscillator strengths of (i) the folded and (ii) the fundamental component. This is much lower than the reported values for the parent compounds $AgGaS_2$ and $AgGaTe_2$. In both cases, the relative oscillator strengths are of the order of unity[12,22] and, in this respect, $AgGaSe_2$ appears closer to the equivalent ZnS-type material.

At room temperature, when the folded component is not resolved, we still used two nearly degenerate oscillators. After running the least-mean-squares fit procedure, this ended with the series of parameters listed in Table II and the reflectivity spectrum shown as a dashed line in Fig. 4(b). A surprising result is the relative strength of the high-energy components. We find about four times the value reported at 20 K which is indicative of a temperature-dependent coupling. We shall come back to this point later, when discussing the Raman data.

### B. Raman data

From Table I, one expects 13 Raman frequencies but, since two modes (one longitudinal and one transverse) must be associated with both infrared-active $\Gamma_4$ and $\Gamma_5$ components, one should observe up to 22 different Raman lines which, of course, should obey different selection rules. In this work, we could only resolve 18. The point is that, like many ternary chalcopyrite compounds, $AgGaSe_2$ does not obey clear selection rules.[22] This does not make the analysis of Raman data a straightforward matter and, in many cases, a close comparison with the infrared spectra has been found necessary.

For clarity we shall start with the Raman exclusive $\Gamma_1$ and $\Gamma_3$ modes. We display, in Fig. 6, experimental data collected in both configurations: $\langle x'|zz|\bar{x}'\rangle$ and $\langle z|xx|\bar{z}\rangle$. The striking feature is the large intensity of the $\Gamma_1$ component which reveals at 181 $cm^{-1}$ [see Fig. 6(a)]. In Fig. 6(b), additional $\Gamma_3$ frequencies reveal also but the scattered intensity is at least one order of magnitude smaller. This is always observed with $AgGaSe_2$: the $\Gamma_1$ component appears, whatever the experimental configuration and, always, dominates the spectrum.

Since Raman scattering is a third-order process which involves two electron-photon and one electron-phonon matrix elements and, because we are only 180 meV below

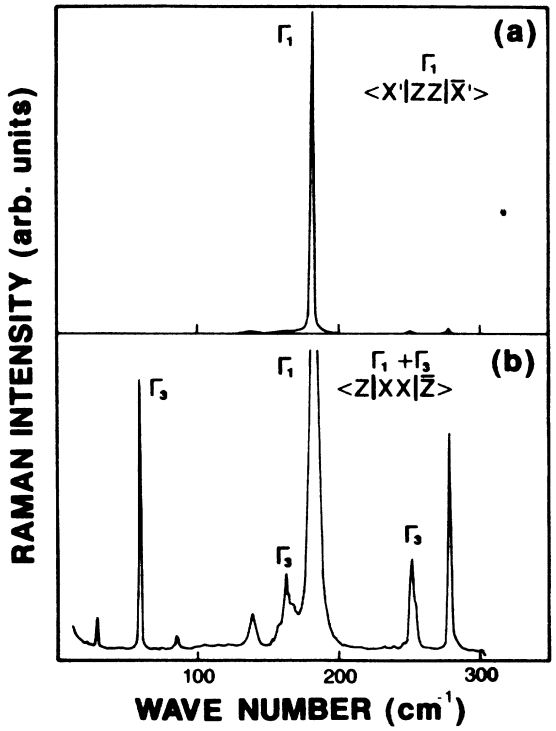


FIG. 6. Typical Raman spectra obtained at 77 K, in the backscattering configuration for $\Gamma_1$ and $\Gamma_3$ modes. In both cases, the exciting frequency was about 180 meV below band gap.

band gap, part of this breaking of the selection rules might be due to resonant enhancement processes. The Raman excitation of a $\Gamma_1$ phonon just requires (i) the direct, first-order allowed, creation of an electron-hole pair in nearly resonant conditions; (ii) the scattering of this electron-hole pair *without* any change of symmetry: and finally, (iii) the direct, first-order allowed, recombination of this electron-hole pair to come back to the crystal ground state. Processes (i) and (iii) are close to resonance: there is only 0.18 eV difference between the incident photon energy (1.65 eV) and the band-gap energy (1.83 eV at 77 K, after Ref. 20). Process (ii) is also a resonant one since the exciton binding energy[20] ($\sim$20 meV) is very close to the phonon energy (22.4 meV). In this case the scattering from one excited state to the ground state of the virtual exciton (electron-hole pair) would be very efficient and symmetry conserving. Concerning the $\Gamma_3$ modes this is no longer true. As already stated, there are two types of $\Gamma_3$ frequencies. First is a $\Gamma_3$ phonon which comes from the $X_3$ longitudinal acoustic branch of the ZnSe-type lattice, and, second, are two $\Gamma_3$ modes which come from the $W_2$ extrema of the Brillouin zone. In both cases, scattering the electron-hole pair signifies that either the hole or the electron *has to change* its wave function from a real (old) $\Gamma$-like one to a new (folded) $\Gamma[X_3]$ or $\Gamma[W_2]$ one. In this case most of the resonance is lost and the interband matrix element which rules the recombination of the electron-hole pair is weaker. As a consequence the intensity drops by about one order of magnitude. Moreover, depending on whether we investigate

$\Gamma_3[X_3]$ or $\Gamma_3[W_2]$ modes, the scattered intensity should be different. In this work, we identify the two $\Gamma_3[W_2]$ modes at 58 and 253 $cm^{-1}$ and the $\Gamma_3[X_3]$ at 160 $cm^{-1}$: obviously, there is a strong difference in Raman intensities. Also found in Fig. 6(b) are additional structures (symmetry forbidden) which will be identified later in this work. This is, again, evidence of the breaking of selection rules which is a constant effect when dealing with chalcopyrites which, in principle, could be reduced by using incidence and collection angles as small as possible. In the present case, even if we used an incidence angle of 20° (collection lens limited) which corresponds[1] in $AgGaSe_2$ to a finite aperture of only 7°, we could not get better data.

Coming now to the $\Gamma_4$ frequencies, we display in Fig. 7

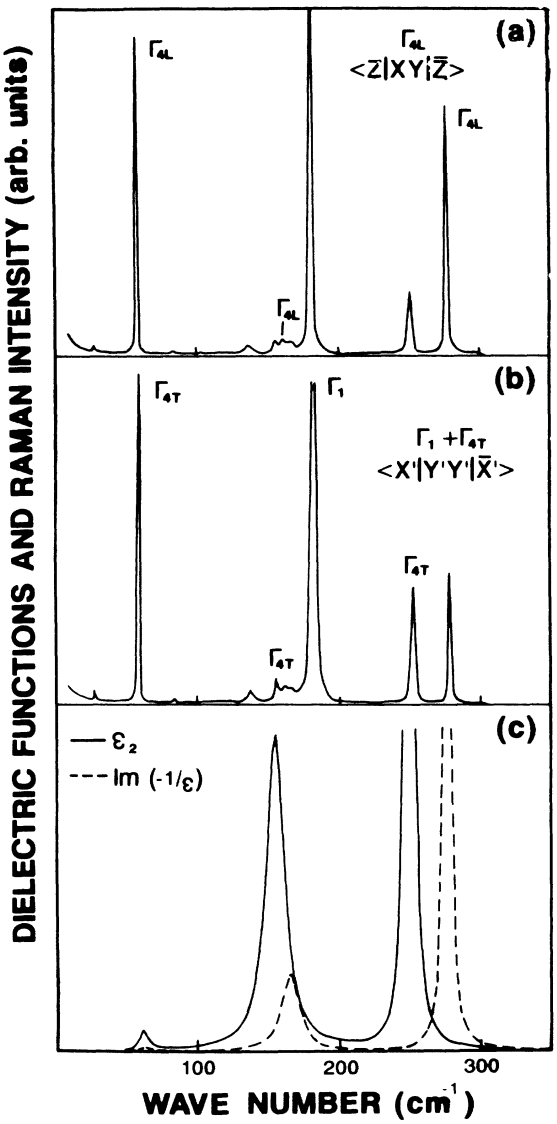


FIG. 7. Same as Fig. 6, but now for the $\Gamma_4$ modes. Also given, for purposes of comparison, is the dielectric function obtained from the oscillator fit analysis. Notice the weak Raman cross section observed around 150 $cm^{-1}$ and the $\Gamma_1$ mode at 181 $cm^{-1}$ on both experimental spectra.

a comparison of the Raman scattering spectra obtained in (a) the $\langle z|xy|\bar{z}\rangle$ configuration, which selects $\Gamma_{4L}$ modes, and (b) the $\langle x'|y'y'|\bar{x}'\rangle$ configuration, which allows us to observe $\Gamma_1$ and $\Gamma_{4T}$ modes; also given are (c) the dielectric functions obtained from our oscillator fit analysis in the polarization $\mathbf{E}\|\mathbf{c}$. Clearly, the two Raman modes observed at 275 and 252 $cm^{-1}$ (77 K) are the longitudinal and transverse frequencies associated with the high-energy $\Gamma_4[\Gamma_{15}]$ component. The second infrared-active band corresponds with much weaker Raman intensities. We observe the longitudinal mode at 161 $cm^{-1}$ and the transverse one at 155 $cm^{-1}$. Finally, the third component is found at 58 $cm^{-1}$ and no longitudinal-transverse splitting could be resolved. From the consideration of Fig. 1, we know already that two partner modes (of $\Gamma_3$ and $\Gamma_4$ symmetry) originate from the same $W_2$ representations of the zinc blende and, from the folded-zone scheme, we know that two such pairs of partner modes should be expected in the low- and high-energy range. From the experimental results of Figs. 6(b) and 7, we notice a much larger effect of the chalcopyrite distortion in the high-energy range. We find almost 100 $cm^{-1}$, as compared to a vanishingly small value for the modes originating from the acoustic branch. This is because, in the first case, the two different bonds participate separately in the two different vibrations (light cations for the $\Gamma_3$ mode and heavy cations for the $\Gamma_4$ mode). On the contrary, in the second case ($\Gamma_3$-$\Gamma_4$ modes coming from the acoustic branch) both types of cations participate in similar fashion in the vibration and, in this case, no experimental splitting could be observed.

Finally, let us investigate the $\Gamma_5$ components. We display in Fig. 8 the corresponding spectra, together with the dielectric functions obtained from our oscillator fit. We expect six longitudinal and transverse frequencies and, from our infrared data, we know already that two lines should be nearly degenerate. Consider first the transverse frequencies [Fig. 8(b)]. In polarization $\langle x'|y'z|\bar{x}'\rangle$, two lines resolve at 251 and 255 $cm^{-1}$. Within experimental uncertainty, this corresponds well with the infrared values. Again we associate the first one (251 $cm^{-1}$) with the $\Gamma_5[\Gamma_{15}]$ transverse component, and the second (255 $cm^{-1}$) with the folded $\Gamma_5[W_4]$ transverse mode. In both cases the anions vibrate along the light cations in very similar ways and our assignment is based only upon consideration of the relative Raman intensities and infrared oscillator strengths (see Table II). Lastly, four lines appear at 162, 137, 84, and 27 $cm^{-1}$. According to the standard ordering expected for ZnS-type materials, they should be associated with $\Gamma_5[X_5]$, $\Gamma_5[W_3]$, $\Gamma_5[W_4]_{ac}$, and $\Gamma_5[X_5]_{ac}$ frequencies, respectively. We notice that the last one agrees well with the low-energy mode observed in Fig. 3(a) and confirms our previous assignment. Finally, for the six $\Gamma_5$ modes effectively observed, only three longitudinal-transverse splittings have been experimentally resolved. The corresponding longitudinal frequencies are 277, 165, and 138 $cm^{-1}$ for the $\Gamma_5[\Gamma_{15}]$, $\Gamma_5[X_5]$, and $\Gamma_5[W_3]$ modes, respectively.

For convenience, we give in Table III a comparison of the Raman and infrared frequencies obtained in this

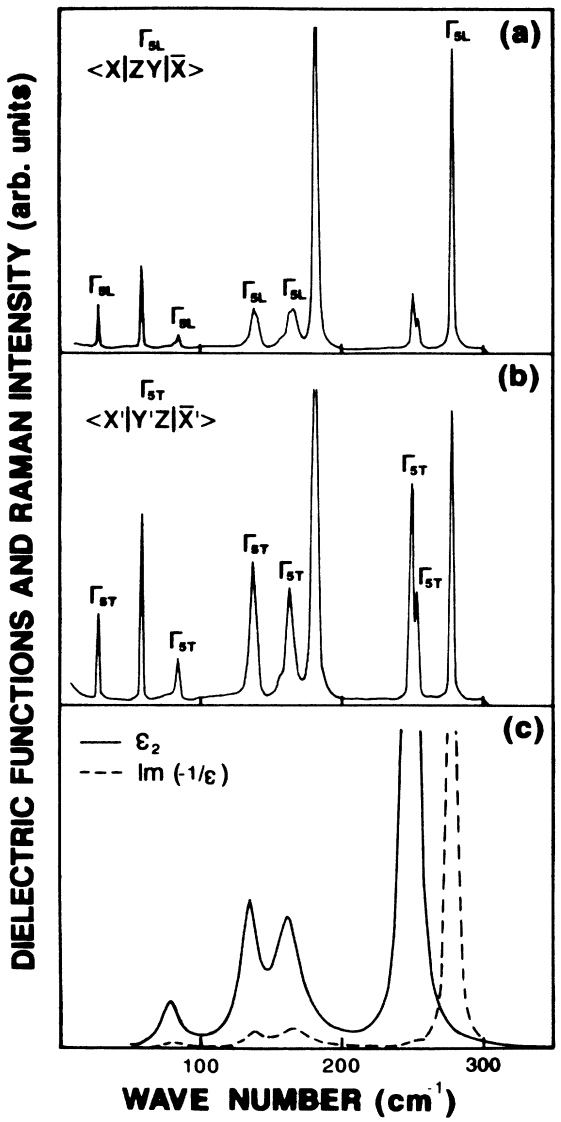


FIG. 8. Same as Fig. 7 but now for the $\Gamma_5$ components. Notice again the $\Gamma_1$ and $\Gamma_{3,4}$ components which appear at 181 and 58 $cm^{-1}$, respectively.

work. We find a very satisfactory agreement concerning all frequencies which have been collected at low temperature (20 and 77 K) but, concerning the infrared spectra which have been collected at room temperature, finite temperature effects can be noticed. Also shown in Table III is the difficulty of assigning modes in $AgGaSe_2$. For instance, the "separation" of the two $\Gamma_3$-$\Gamma_4$ components at 58 $cm^{-1}$ could only be done on the basis of relative intensities with respect to the "forbidden" $\Gamma_5[\Gamma_{15}]_L$ component (compare Figs. 6, 7, and 8) and no high-resolution spectra could separate these two modes.

This is not the case when dealing with the manifold which appears around 250 $cm^{-1}$. In this energy range, five components interplay. They are (i) the two $\Gamma_5[W_4]$ longitudinal and transverse frequencies, (ii) the $\Gamma_5[\Gamma_{15}]$ and $\Gamma_4[\Gamma_{15}]$ transverse frequencies, and (iii) the $\Gamma_3[W_2]$ mode. A high-resolution experiment, in this case, has proven helpful.

Our experimental spectra are shown in Fig. 9. The experimental resolution was 0.7 $cm^{-1}$ and we have used a xenon calibration line to check all absolute values. First is an $\langle x'|zy'|\bar{x}'\rangle$ configuration, where only $[\Gamma_5]_T$ modes are allowed. The corresponding spectrum clearly shows two lines, at 251 and 255 $cm^{-1}$, and a large dip separates these lines. Next is a $\langle z|xx|\bar{z}\rangle$ configuration where, in this energy range, only the $\Gamma_3$ mode is allowed [Fig. 9(b)]. The dominant feature is found at 253 $cm^{-1}$. Finally, in Fig. 9(c), is a $\langle x'|y'y'|\bar{x}'\rangle$ configuration where, again, in this energy range, only the $\Gamma_4$ mode is allowed. In this case the dominant feature appears at 252 $cm^{-1}$. We have also investigated the $\langle x|zy|\bar{x}\rangle$ configuration. We expected to find the longitudinal $\Gamma_5[W_4]$ mode but no clear experimental feature could be found. From infrared data plotted in Fig. 8(c), we know that the corresponding intensity should be very small; indeed, only one weak shoulder [similar to the one already displayed in Fig. 9(a)] appeared on the high-energy side of the $\Gamma_5[\Gamma_{15}]_T$ component, below the $\Gamma_5[W_4]_T$ frequency. It suggests the possibility of a *negative* LO-TO splitting, similar to the one already observed in $\alpha$-quartz[19,23] and $\alpha$-$AlPO_4$.[19] In both cases, this is because a weak mode falls between two longitudinal and transverse frequencies associated with a vibration of the same symmetry. The infrared dispersion, because of both TO frequencies, on the one hand, and LO frequencies, on the other hand, results in a negative LO-TO splitting for the intermediate vibration. In our case

TABLE III. Summary of experimental results obtained in this work. Note $(\ )_a$ are absorption data (see text).

| | Frequency ($cm^{-1}$) | | |
|---|---|---|---|
| Mode | Infrared (300 K) | Raman (77 K) | Infrared (20 K) |
| $\Gamma_1[W_1]$ | | 181 | |
| $\Gamma_3[W_2]$ | | 253 | |
| $\Gamma_3[X_3]$ | | 160 | |
| $\Gamma_3[W_2]_{ac}$ | | 58 | |
| | 275.5 (L) | 275(L) | |
| $\Gamma_4[\Gamma_{15}]$ | 249.5(T) | 252(T) | |
| | 165 (L) | 161(L) | |
| $\Gamma_4[W_2]$ | 154.5(T) | 155(T) | |
| | 63 (L) | | |
| $\Gamma_4[W_2]_{ac}$ | 62.5(T) | 58(T+L) | $(57)_a$ |
| | 278.5(L) | 277(L) | 276 (L) |
| $\Gamma_5[\Gamma_{15}]$ | 248 (T) | 251(T) | 249.5(T) |
| | 250 (L) | | |
| $\Gamma_5[W_4]$ | 251 (T) | 255(T) | 252.1(T) |
| | 165 (L) | 165(L) | 164 (L) |
| $\Gamma_5[X_5]$ | 162.5(T) | 162(T) | 162 (T) |
| | 137 (L) | 138(L) | 136 (L) |
| $\Gamma_5[W_3]$ | 135 (T) | 137(T) | 135 (T) |
| | 80 (L) | | |
| $\Gamma_5[W_4]_{ac}$ | 79 (T) | 84(T+L) | $(84)_a$ |
| $\Gamma_5[X_5]_{ac}$ | | 27(T) | $(26)_a$ |

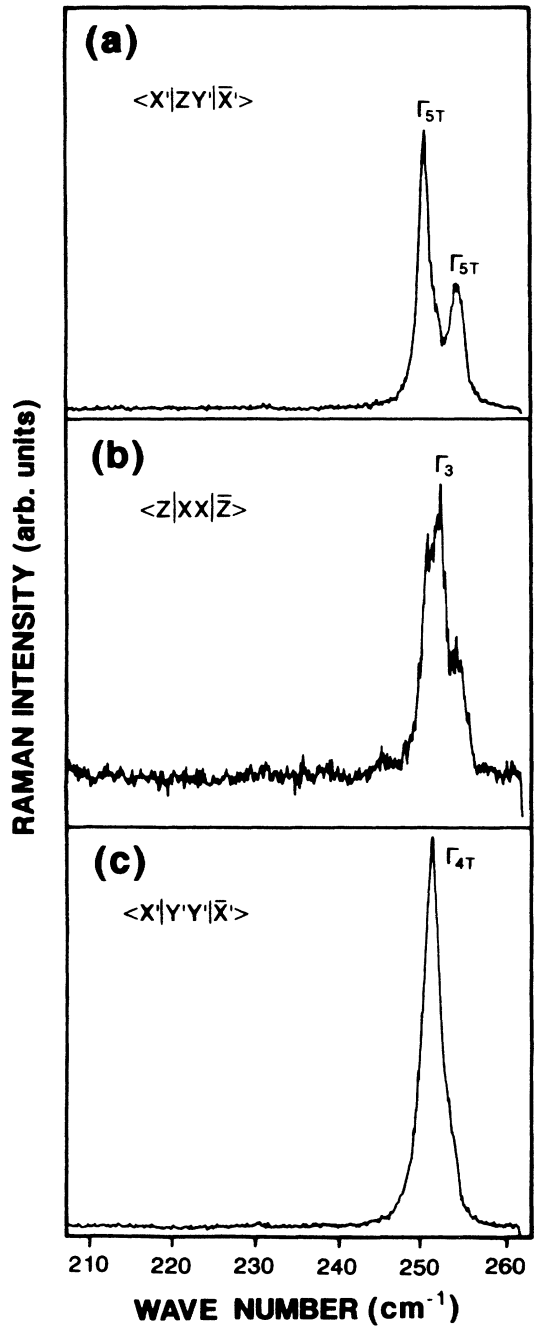


FIG. 9. High-resolution spectra observed around 250 $cm^{-1}$. Please notice the large intensity of the two $\Gamma_5$(TO) components. This is indicative of a larger admixture when compared with the infrared reflectivity spectrum of Fig. 5 (temperature change from 77 to 20 K).

we believe in a slightly different scheme. At finite temperature, both TO frequencies (nearly degenerate) couple. This results in a large transfer of oscillator strength which explains (i) the change in infrared intensities between 20 and 300 K (see Table II) and (ii) the large Raman cross section of both transverse components in Fig. 8(a). The two LO frequencies are too far apart and do not couple much. This explains the small Raman intensity of the weak LO component.

## V. MACROSCOPIC EFFECTIVE CHARGES

In polar crystals, the macroscopic effective charges determine the magnitude of the LO-TO splitting. Typical values range from about 40 $cm^{-1}$, for the $\Gamma_{15}$ mode of ZnSe (Ref. 8) or the $\Gamma_4$ and $\Gamma_6$ modes of CdSe,[24] to about 25 $cm^{-1}$ for the $\Gamma_4[\Gamma_{15}]$ and $\Gamma_5[\Gamma_{15}]$ modes of $AgGaSe_2$ (see Table III). A detailed discussion would require a knowledge of the eigenvectors for all infrared-active components, but a simple estimate can be done if we follow the path of Scott[25] for aluminum phosphate.

We start from the review paper by Lauwers[26] and write, in the rigid-ion approximation,

$$\sum_{j(\Gamma_4,\Gamma_5)} (\nu_{\mathrm{LO},j}^2 - \nu_{\mathrm{TO},j}^2) = \frac{1}{\pi V}\left[\frac{4(Z_{\mathrm{Se}}^*)^2}{m_{\mathrm{Se}}} + \frac{2(Z_{\mathrm{Ag}}^*)^2}{m_{\mathrm{Ag}}} + \frac{2(Z_{\mathrm{Ga}}^*)^2}{m_{\mathrm{Ga}}}\right] \quad (1)$$

where $j$ sums over the three $\Gamma_4$ and six $\Gamma_5$ modes; $V$ is the volume of the unit cell and $Z_A^*$ is the effective charge of atom $A$. Using data listed in Table III, this gives one equation and three unknown parameters. One additional relation can be obtained from the expression of the lattice neutrality:

$$4Z_{\mathrm{Se}}^* + 2Z_{\mathrm{Ag}}^* + 2Z_{\mathrm{Ga}}^* = 0 \quad (2)$$

and a reasonable value for $Z_{\mathrm{Se}}^*$ can be deduced from the consideration of the two binary compounds ZnSe and CdSe. From the data listed in Ref. 8, we get

$$Z_{\mathrm{Se}}^*(\mathrm{ZnSe}) = 0.83$$

and, from results listed in Refs. 24 and 26:

$$Z_{\mathrm{Se}}^*(\mathrm{CdSe}) = 0.9 \ .$$

This gives an averaged value of about 0.85 which, combined with the results of Eqs. (1) and (2), gives

$$Z_{\mathrm{Ga}}^* = 1.03 \quad \text{and} \quad Z_{\mathrm{Ag}}^* = 0.67 \ .$$

This means that, for silver atoms, the electronic contribution to the LO-TO splitting of the zone-center modes is about $\frac{2}{3}$ of that of the gallium atoms. This is about two times the value that one would expect, neglecting all electronic charge transfer and considering only the valence electrons. As a matter of fact there is, of course, a transfer of valence charge from gallium to silver in order to come closer to the one (two electrons per bonds) characteristic of ZnS-type materials. This results[4] in a lower bond charge on the longer bond (Ga—Se) and a higher bond charge on the shorter bond (Ag—Se). In this case, assuming that the repartition of the valence charge is similar to the one found for the repartition of the effective charges in this work, one would get, for $AgGaSe_2$,

$$e^*(\mathrm{Ag}) = 1.6 \quad \text{and} \quad e^*(\mathrm{Ga}) = 2.4 \ .$$

It indicates that, in order to screen the point-ion perturbation, about 0.3 electrons per bond had to transfer from gallium to silver through the common anions.

## VI. CONCLUSION

Performing, first, infrared studies in the spectral range 15–500 $cm^{-1}$, both at room and liquid-helium temperature, and collecting, second, complementary Raman data at 77 K, under nearly resonant conditions, we could resolve all zone-center modes of $AgGaSe_2$. We have found that the 13 optically active frequencies range in three bands. First, in a very narrow range between 251 and 255 $cm^{-1}$, are four modes. They have $1\Gamma_3+1\Gamma_4+2\Gamma_5$ symmetry. Next, in an intermediate region extending from 180 to 135 $cm^{-1}$, are five modes with $1\Gamma_1+1\Gamma_3+1\Gamma_4+2\Gamma_5$ symmetry. This ordering departs from the predictions of the folded-zone scheme and outlines the peculiarities of the chalcopyrite structure with respect to the corresponding ZnS-type material. Finally, at much lower energy, we find a last series of four modes. They range from 25 to 85 $cm^{-1}$ and come from the dispersion of the acoustic branches. They are associated with $1\Gamma_3+1\Gamma_4+2\Gamma_5$ symmetry.

## ACKNOWLEDGMENTS

During the course of this work, we benefited from much support. We thank R. Feigelson (Stanford University, Palo Alto, CA) for kindly providing us with high-quality single crystals; M. Galtier, from the Groupe de Dynamique des Phases Condensées (GDPC) for expert assistance with the infrared Fourier-transform (IRFT) spectrometer and C. Montaner, also from the GDPC, for the loan of the low-temperature reflectivity apparatus; we used a least-mean-squares fit program written by A. Goullet (GES) and, finally, we acknowledge M. Cardona and the Max Planck Institute (Stuttgart, Germany) for the use of their Raman scattering facilities.

[1]G. D. Boyd, H. M. Kasper, J. H. McFee, and F. G. Storz, IEEE J. Quantum Electron. **QE-8**, 900 (1972); also see G. D. Boyd, E. Buehler, F. G. Storz, and J. H. Wernick, *ibid.* **QE-8**, 419 (1972).

[2]W. Hörig, H. Neumann, H. Sobota, B. Schumann, and G. Kühn, Thin Solid Films **48**, 67 (1978); also see Ref. 4.

[3]J. L. Shay and J. H. Wernick, *Ternary Chalcopyrite Semiconductors: Growth, Electronic Properties and Applications* (Pergamon, New York, 1975).

[4]J. E. Jaffe and A. Zunger, Phys. Rev. B **29**, 1882 (1984); also see **28**, 5822 (1983).

[5]G. Nilson and G. Nelin, Phys. Rev. B **3**, 364 (1971).

[6]G. Nilson and G. Nelin, Phys. Rev. B **6**, 3777 (1972).

[7]D. Strauch and B. Dorner (unpublished).

[8]J. C. Irwin and J. Lacombe, Can. J. Phys. **50**, 2596 (1972).

[9]J. P. Van der Ziel, A. E. Meixner, H. M. Kasper, and J. A. Ditzenberger, Phys. Rev. B **9**, 4286 (1974).

[10]A. Miller, G. D. Holah, W. D. Dunnet, and G. W. Iseler, Phys. Status Solidi B **78**, 569 (1976).

[11]B. Hennion, F. Moussa, G. Pepy, and K. Kunc, Phys. Lett. **36A**, 376 (1971).

[12]G. Kanellis and K. Kampas, J. Phys. (Paris) **38**, 833 (1977).

[13]L. Artus, J. Pascual, A. Goullet, and J. Camassel, Solid State Commun. **69**, 753 (1989).

[14]P. N. Keating, Phys. Rev. **145**, 637 (1966).

[15]R. M. Martin, Phys. Rev. B **1**, 4005 (1970).

[16]E. O. Kane, Phys. Rev. B **31**, 7865 (1985).

[17]M. Bettini, Phys. Status Solidi B **69**, 201 (1975).

[18]A. Goullet, P. Rouquette, J. Camassel, J. Pascual, and J. C. Jumas, Solid State Commun. **62**, 187 (1987).

[19]J. Camassel, A. Goullet, and J. Pascual, Phys. Rev. B **38**, 8419 (1988).

[20]L. Artus and Y. Bertrand, Solid State Commun. **61**, 733 (1987).

[21]J. L. Duarte, J. A. Sanjurjo, and R. S. Katiyar, Phys. Rev. B **36**, 3368 (1987); also see A. Goullet, J. Camassel, L. Martin, J. Pascual, and E. Phillipot, *ibid.* **40**, 5750 (1989).

[22]G. D. Holah, J. S. Webb, and H. Montgomery, J. Phys. C **7**, 3875 (1974).

[23]S. M. Shapiro and J. D. Axe, Phys. Rev. B **6**, 2420 (1972); also see C. T. Kirk, *ibid.* **38**, 1255 (1988).

[24]V. G. Plotnichenko, Yu. A. Mityagin, and I. K. Vodop'Yanov, Fiz. Tverd. Tela (Leningrad) **19**, 2706 (1977) [Sov. Phys.—Solid State **19**, 1584 (1977)].

[25]J. F. Scott, Phys. Rev. B **4**, 1360 (1971).

[26]H. A. Lauwers, J. Phys. Chem. Solids **49**, 173 (1988).